Fireside Corrosion of Alloys for Combustion Power Plants*

K. Natesan
Argonne National Laboratory, 9700 South Cass Avenue, Argonne, IL 60439
E-mail: natesan@anl.gov; Telephone: (630) 252-5103; Fax: (630) 252-3604

A. Purohit and D. L Rink
Argonne National Laboratory, 9700 South Cass Avenue, Argonne, IL 60439
E-mail: purohit@anl.gov; Telephone: (630) 252-5949; Fax: (630) 252-3604

Manuscript

A program on fireside corrosion is being conducted at Argonne National Laboratory to evaluate the performance of several structural alloys in the presence of mixtures of synthetic coal ash, alkali sulfates, and alkali chlorides. Candidate alloys are also exposed in a small-scale coal-fired combustor at the National Energy Technology Laboratory in Pittsburgh. Experiments in the present program, which addresses the effects of deposit chemistry, temperature, and alloy chemistry on the corrosion response of alloys, were conducted at temperatures in the range of 575-800°C for time periods up to ≈1850 h. Alloys selected for the study included HR3C, 310TaN, HR120, SAVE 25, NF709, modified 800, 347HFG, and HCM12A. In addition, 800H clad with Alloy 671 was included in several of the exposures. Data were obtained on weight change, scale thickness, internal penetration, microstructural characteristics of corrosion products, mechanical integrity, and cracking of scales. Results showed that relationship of corrosion rates to temperature followed a bell-shaped curve, with peak rates at ≈725°C, but the rate itself was dependent on the alloy chemistry. Several alloys showed acceptable rates in the sulfate-containing coal-ash environment; but NaCl in the deposit led to catastrophic corrosion at 650 and 800°C.

Background

Conceptual designs of advanced combustion systems that utilize coal as feedstock must include improved thermal efficiency and significant reduction in release of sulfur oxides, nitrogen oxides, and carbon dioxide. Such systems require materials and components that are capable of operating at much higher temperatures than those found in current coal-fired power plants. Component reliability and long-term, trouble-free performance of structural materials for these systems necessitate development/evaluation of materials in simulated coal-combustion environments. Apart from the environmental aspects of the effluent from coal combustion, one concern from the systems standpoint is the aggressiveness of the combustion environment toward boiler structural components such as steam superheaters and reheaters.

Recently, the U.S. Department of Energy has started to reevaluate coal-fired steam generation plants and, in particular, the designs based on supercritical and ultra supercritical steam conditions. The ultimate goal of the staged development of power systems is to change steam pressure and temperature from the current values of 16.5-24 MPa (2400-3500 psig) and 540°C (1000°F), respectively, to 34.5 MPa (5000 psig) and 650°C (1200°F). Development of a revolutionary boiler design for U.S. markets, based on superheater/reheater temperatures >760°C, is also proposed. The higher steam temperature is expected to lead to another 2-3% increase in efficiency over a 700°C design, thus improving fuel usage and CO_2 emissions [1].

Fireside metal wastage in conventional coal-fired boilers can occur by gas-phase oxidation or deposit-induced liquid-phase corrosion. The former can be minimized by using materials that are resistant to oxidation at the service temperatures of interest. On the other hand, deposit-induced corrosion of materials is an accelerated type of attack, influenced by the vaporization and condensation of small amounts of impurities such as sodium, potassium, sulfur, chlorine, and vanadium (or their compounds) that are present in the coal feedstock. At the temperatures of interest in advanced combustion systems,

*Work supported by the U.S. Department of Energy, Office of Fossil Energy, Advanced Research Materials Program, Work Breakdown Structure Element ANL-4, under Contract W-31-109-Eng-38.

mixtures of alkali sulfates, along with alkali chlorides, will dominate the fireside deposit, and viable structural alloys must be resistant to attack by such deposits. The temperature regimes in which this corrosion occurs are summarized in Figure 1.

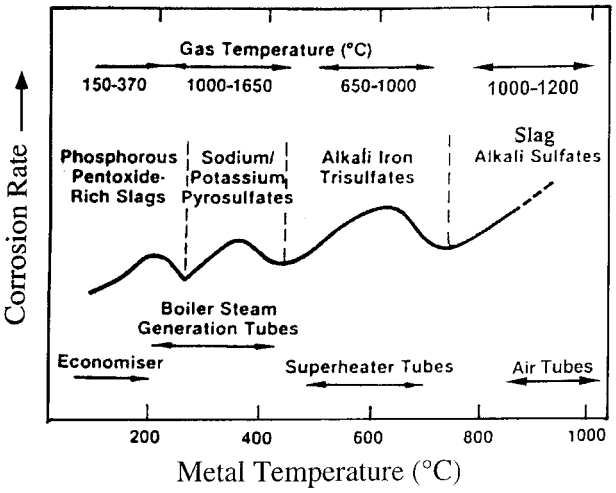

Figure 1. Regimes of fireside corrosion in coal-fired boilers.

Because most of the materials for application in boiler tubes are iron-based alloys, and because the mobility of iron from the alloy substrate to the scale/gas interface is fairly rapid, considerable attention has been given to understanding the formation of alkali-iron trisulfates and their role in the corrosion of steam superheaters in conventional boiler systems [2-4]. The effect of boiler deposits on the corrosion of structural materials has been fairly well established by Reid [2]. A general mechanism and sequence of events for alkali-iron-trisulfate-induced corrosion of iron-based materials begins with the formation of an oxide film on the metal surface, and/or oxidation of pyrite in the coal to form iron oxide and sulfur dioxide/sulfur trioxide gases. Alkali sulfates that originate from alkalis in the coal and sulfur oxides in the furnace atmosphere are deposited over the oxide scale on superheater materials. Eventually, because of an increasing temperature gradient, the outer surface of the alkali sulfate layer becomes sticky, and particles of fly ash are captured. With further increase in temperature, thermal dissociation of sulfur compounds in the ash releases SO_3, which migrates toward the cooler metal surface while a layer of slag forms on the outer surface. With more ash in the outer layer, the temperature of the sulfate layer falls, and reaction occurs between the oxide scale and SO_3, to form alkali-iron trisulfate. With this removal of the oxide scale, the metal oxidizes further. Deslagging due to temperature excursions or soot blowing to remove the deposits exposes the alkali-iron trisulfates to higher temperatures and leads to dissociation of sulfate and generation of SO_3 for further attack of the metal.

In advanced combustion systems, as the steam temperature increases further, the metals in the superheater regions will be subjected to much higher temperature, and alkali sulfate and coal ash will be the predominant deposit. Several factors, including sulfur, alkali, chlorine in coal feedstock, excess air level during the combustion process, and metal temperature, determine the extent of corrosion of superheater materials in coal-fired boilers. The objective of the present work is to evaluate the corrosion performance of state-of-the-art candidate materials in coal ash, alkali sulfate, and alkali chloride environments at temperatures in the range of 650-800°C. The experimental program is aimed at developing a scientific understanding of corrosion mechanisms as a function of alloy composition and deposit chemistry, and at quantitatively determining the scaling and internal penetration of the alloys.

Experimental Procedure

Several alloys, both ASME-coded and uncoded, were selected for corrosion evaluation; however, only eight of the alloys are included in this paper. The compositions of the selected alloys are listed in Table 1. Among those selected, HCM12A is a super ferritic alloy in which creep strengthening is obtained by both solution strengthening (W and Mo) and precipitation strengthening (V, Nb, and N). The alloy contains Cu (instead of Ni) to stabilize the long-term creep strength and to minimize δ-ferrite. The included austenitic alloys were broadly based on 18-20Cr and 20-25Cr steels. Super 304H, 347HFG, and

NF709 fall into 18-20Cr steels, with improved creep strength achieved by addition of Nb and/or Ti. HR3C, 310TaN, and SAVE 25 fall into 20-25Cr steels, with improved creep strength achieved by addition of Nb, Ti, Ta, and N. Modified 800 is the Alloy 800 base, with additions of the strengthening elements Nb, V, N, and B. HR120 is a Fe-Ni-Cr alloy with additions

Table 1. Nominal composition (in wt.%) of alloys selected for corrosion study

Material	C	Cr	Ni	Mn	Si	Mo	Fe	Other
HCM12A	0.10	12	0.3	0.5	0.3	0.4	Bal	W 2.0, V 0.2, Nb 0.05, Cu 0.9, N 0.05
Super 304H	0.10	18	9	1.0	0.3	-	Bal	Nb 0.45, Cu 3.0, N 0.09
347HFG	0.08	18	11	2.0	1.0	-	Bal	Nb + Ta = 10 x C min
HR3C	0.06	25	20	1.2	0.4	-	Bal	Nb 0.45, N 0.2
310TaN	0.05	25	20	1.0	0.2	-	Bal	Ta 1.5, N 0.2
NF709	0.07	20	25	1.0	0.6	1.5	Bal	Ti 0.6, Nb 0.2, N 0.18, B 0.004
SAVE 25	0.10	23	18	1.0	0.4	-	Bal	Nb 0.45,, W 1.5, Cu 3.0, N 0.2
Modified 800	0.10	20	30	1.5	0.2	1.5	Bal	Ti 0.25, Nb 0.25, V 0.05, N 0.03, B 0.004
HR120	0.05	25	37	0.7	0.6	2.5	Bal	Co 3, W 2.5, N 0.2, Cu 0.18, B 0.004, Al 0.1, Nb 0.7
671-clad 800H								
671	0.05	48	Bal	0.02	0.2	-	0.2	Ti 0.4
800	0.05	21	32	0.5	0.2	-	Bal	Ti 0.4, Al 0.4

of primarily Co, W, and Nb. In addition, specimens of 800H clad with Alloy 671 were also included in the study. The specimens of alloys, in the form of coupons ≈8-10 x 10 x 2 mm, were wet-ground with 600-grit SiC paper; they were identified by letters stamped at the corner of the coupons and were thoroughly degreased in clean acetone, rinsed in water and dried.

A schematic diagram of the experimental setup used for the isothermal corrosion tests is shown in Figure. 2. The experiments were conducted in a horizontal resistance-heated furnace that contained a 55-mm-i.d. x 3-mm-wall alumina reaction tube. The specimen was laid flat on a tray in the constant-temperature region of the chamber and was covered with a synthetic mixture of coal ash, alkali sulfates and NaCl. The synthetic coal ash consisted of a mixture of reagent-grade SiO_2, Al_2O_3, and Fe_2O_3 in the ratio of 1:1:1 by weight. The alkali sulfate mixture consisted of Na_2SO_4 and K_2SO_4 in the ratio of 1:1 by weight. Two types of deposits were used in the corrosion experiments. In the first, ash and sulfate were mixed in the ratio of 90:10 by weight; in the second, ash, sulfate, and NaCl were mixed in the ratio of 85:10:5 by weight. The temperature was measured by a thermocouple inserted into an alumina thermowell that was fed through an opening in the flange of the reaction chamber. The specimens were exposed at temperatures of 575, 650, 725, and 800°C for time periods in the range of 336-1852 h. The experiments were generally stopped after either 168 or 336 h, and the specimens were cooled to room temperature, cleaned of the ash by brushing, and weighed. Specimen exposures were continued with a fresh deposit mixture. Temperature was controlled to within ≈3°C in the vicinity of the specimens. A gas mixture of high-purity air that contained 1 vol.% SO_2 was fed through a Pt catalyst maintained at elevated temperature to ensure SO_2/SO_3 equilibrium in the gas mixture near the specimens.

Upon completion of the corrosion kinetics experiments, the specimens were examined by optical metallography and a scanning electron microscope (SEM) equipped with energy–dispersive X–ray analyzer. Optical examination of cross sections of exposed specimens, and analyses with the SEM, were used to identify the morphological features of corrosion-product phases in the scale layers and to establish the thickness of scales and depth of intergranular penetration, if any, of the alloys and cladding.

Results and Discussion

At each exposure temperature, specimens of various alloys were exposed to a mixture of coal ash and alkali sulfate for 168 h, after which the specimens were retrieved, cleaned of deposit, and weighed. Subsequently, the exposures were continued with

a fresh deposit mixture for another 168 h. The procedure was repeated several times at various temperatures to accumulate weight change data, which was plotted as a function of exposure time to develop a corrosion rate at each temperature for each alloy. In general, the weight change followed linear kinetics for all of the alloys. At temperatures of 575, 650, and 725°C, most of the alloys lost weight, and the losses were strongly dependent on the alloy composition. At 800°C, several of the alloys gained weight, and a few of them lost weight, but not to the same extent as observed at 725°C.

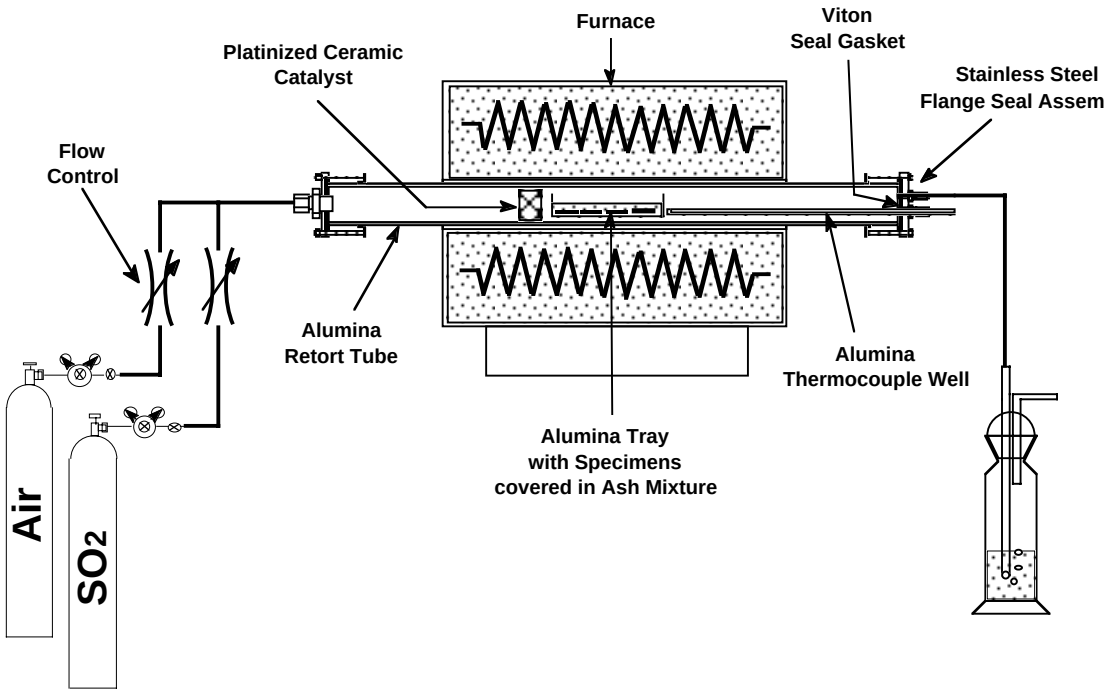

Figure 2. Schematic diagram of furnace assembly, and gas flow, and specimen arrangement used for corrosion experiments.

Figure 3 shows the weight change data for several alloys tested at temperatures between 575 and 800°C. The results indicate that the weight loss rates increase with temperature up to 725°C and decrease to low values at 800°C. In fact, several of the alloys showed either negligible weight loss and or gained weight after exposure at 800°C. The corrosion rates followed a bell-shaped curve with peaks near 725°C for all of the alloys used in this study. The data shown in Figure 3 should only be used qualitatively, because the weight loss rates can be affected by the removal of scales during removal of coal ash deposit from the specimen surface, even though every effort was made to remove only the ash deposits by brushing. Generally, the scales adhered more to some alloys than others, and caution should be exercised in using this information for corrosion allowance for components. Figure 3 also shows the weight loss rates for several alloys at 650 and 800°C, obtained when exposed in a deposit mixture that contained 5 wt.% NaCl. Based on the weight loss data, the presence of NaCl in the deposit has little effect on the corrosion rate at 650°C. Most of the alloys used in this study exhibited similar weight loss rates after exposure in deposits with and without NaCl. On the other hand, at 800°C, several alloys exhibited accelerated corrosion in the presence of deposit that contained NaCl, when compared with the rates observed for the same alloys in the absence of NaCl.

Figure 4 shows total corrosion (scale thickness plus penetration) for several alloys after exposure at 650, 725, and 800°C in an environment that contained coal ash and alkali sulfate. Results show that at 650°C, alloys such as 347HFG, SAVE25, and 800H exhibited total corrosion rate <0.2 mm/y and all of the other alloys showed rates ≤0.44 mm/y. At 725°C, the corrosion rate for all of the alloys increased, and several of them exhibited dramatic increase. For example, the rates for SAVE25 and modified 800H were 2.1 and 1.65 mm/y, respectively. At 800°C, the corrosion rates for several alloys slightly decreased from the values obtained at 725°C. Figure 5 shows the plot of corrosion rate as a function of temperature for several alloys used in this study. Results indicate that NF709 was the superior performing alloy, with rates of 0.26, 0.25, and 0.55 mm/y at 650, 725, and 800°C, respectively. The corresponding values for 310 TaN were 0.43, 0.50, and 0.55 mm/y, respectively.

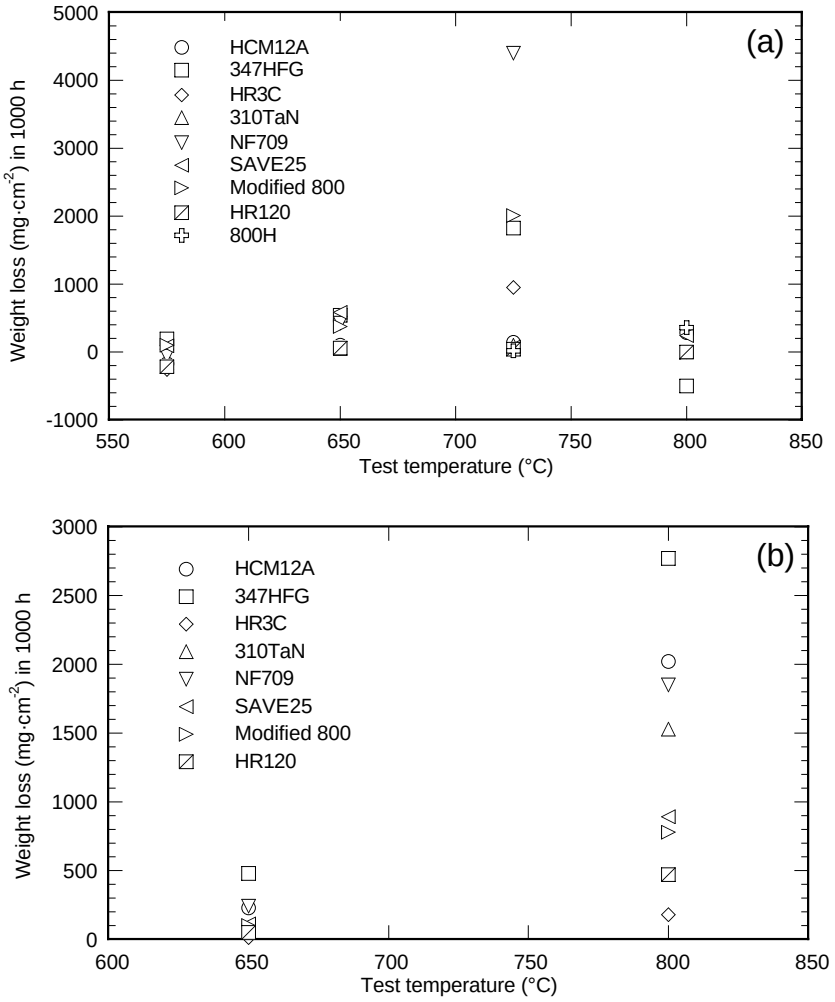

Figure 3. Weight loss data for several alloys after exposure in mixtures of (a) synthetic coal ash and alkali sulfates and (b) synthetic coal ash, alkali sulfates, and NaCl at temperatures between 575 and 800°C.

The effect of NaCl in the deposit mixture on the corrosion performance was evaluated by adding 5 wt.% NaCl to the ash and alkali sulfate mixture. Experiments were conducted at 650 and 800°C. Figure 6 shows the total corrosion (scaling plus penetration) rate for the alloys at 650 and 800°C with and without NaCl. Results indicate that NaCl accelerated corrosion in all of the alloys used in this study. NF709, the best performing alloy in the absence of NaCl, showed corrosion rates of 2 and 15 mm/y at 650 and 800°C in the presence of NaCl. The best performing alloy in environments with and without NaCl was HR3C. The corrosion rates of this alloy were 0.37 and 0.7 mm/y at 650°C, in environments without and with NaCl. Additional work is planned to evaluate the corrosion performance of these materials at 725°C and with a less NaCl in the deposit.

The causes for accelerated corrosion in the heat resistant alloys in the presence of NaCl are two fold. The presence of NaCl in the deposit mixture establishes within the deposit mixture a Cl activity, which can attack the carbides that are present in the alloy as strengtheners. Furthermore, the Cl activity in the deposit near the alloy can be high enough to form volatile chlorides of Fe, Cr, and Al (if present in the alloy). The volatile chlorides lead to a porous microstructure in the alloy with virtually no scale development to protect the alloy. Figures 7 and 8 show the SEM microphotographs of cross sections of modified 800H and SAVE 25 after exposure at 650°C in deposits with and without NaCl.

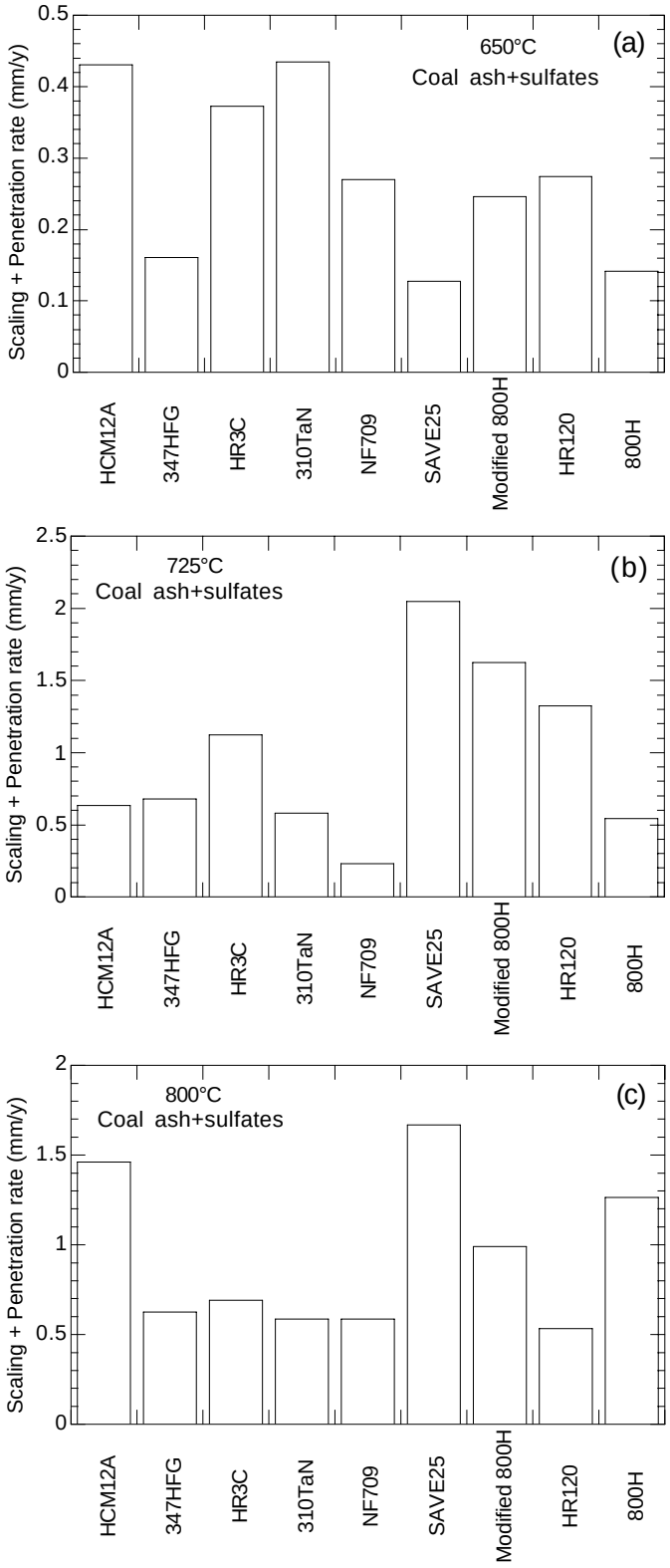

Figure 4. Scaling rate plus penetration rate for several alloys after exposure at (a) 650, (b) 725, and (c) 800°C in mixture of synthetic coal ash and alkali sulfates.

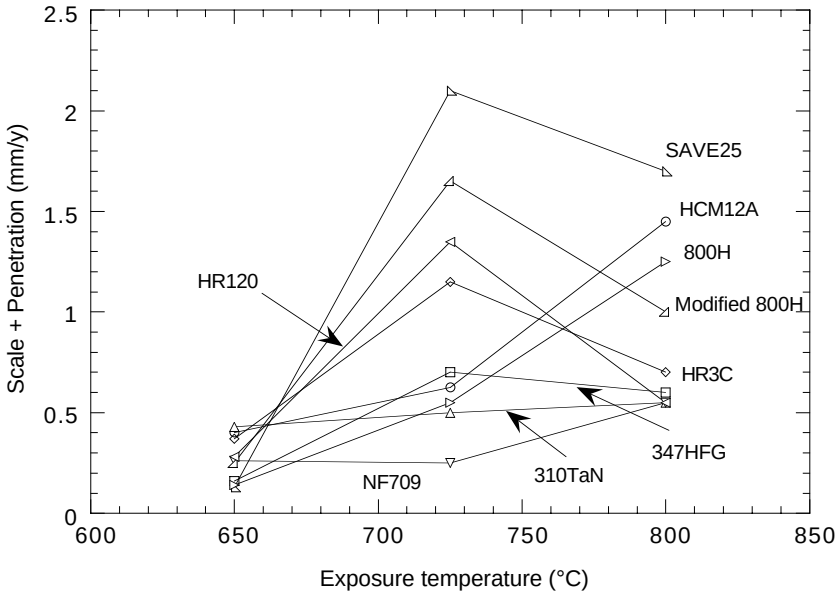

Figure 5. Scaling rate plus penetration rate for several alloys as function of exposure temperature.

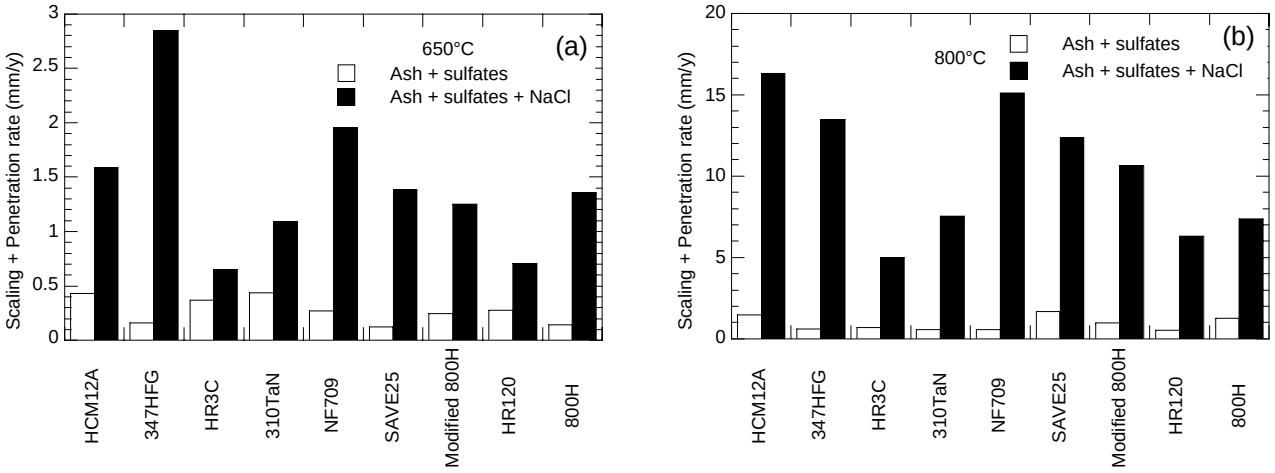

Figure 6. Scaling rate plus penetration rate for several alloys after exposure at (a) 650°C and (b) 800°C in presence of deposits with and without NaCl.

Specimens of Alloy 800H clad with Alloy 671 were also tested at several temperatures and in deposits with and without NaCl. Figure 9 shows SEM photomicrographs of a cross section of the clad alloy after exposure at 650°C in a mixture of coal ash and alkali sulfate. It is evident that Alloy 800 was subjected to significant corrosion whereas the clad alloy developed a thin oxide scale and experienced minimal corrosive attack. The SEM photomicrograph in Figure. 9c shows that the clad alloy far away from the interface developed an ≈3-μm-thick oxide layer that was adherent and protective against corrosion of the underlying alloy. Figure 10 shows SEM photomicrographs of 800H clad with 671 after exposure at 800°C to a mixture of coal ash and alkali sulfate. We plan to evaluate several Ni-base alloys in ash mixtures that contain both alkali sulfate and alkali chloride. Nickel-base alloys are expected to resist chloride attack because the vapor pressure of $NiCl_2$ will be much lower than that of Fe, Cr, and Al chlorides for the same Cl activity and gas temperature [5, 6].

Summary

Fireside corrosion is a major issue when selecting materials for advanced steam-cycle systems. We have conducted studies at Argonne National Laboratory to evaluate the corrosion performance of several candidate materials in coal ash environments. The laboratory tests simulated the combustion atmosphere of advanced steam-cycle systems and two deposit chemistries,

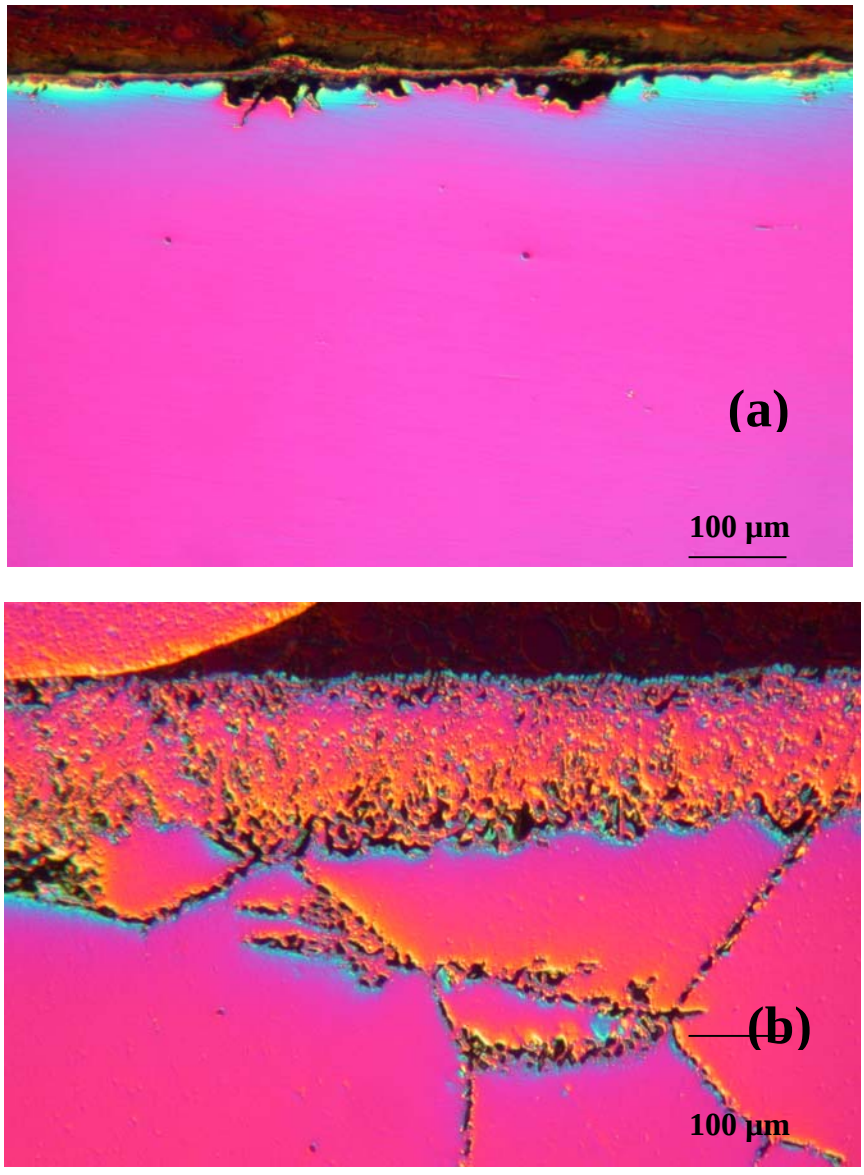

Figure 7. SEM photomicrographs of modified 800H alloy after exposure at 800°C for (a) 672 h in coal ash and alkali sulfate and (b) 336 h in coal ash, alkali sulfate, and NaCl mixture.

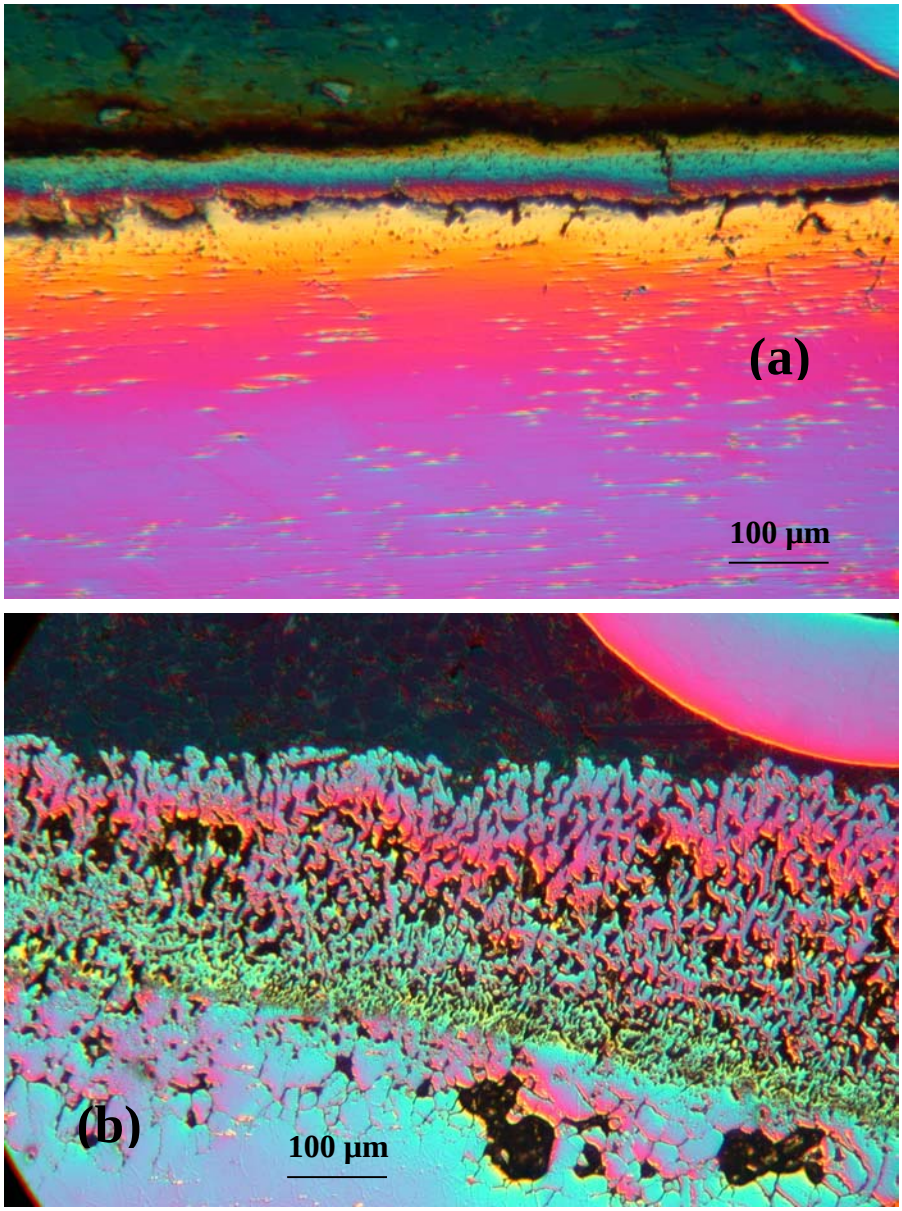

Figure 8. SEM photomicrographs of SAVE25 alloy after exposure at 800°C for (a) 672 h in coal ash and alkali sulfate and (b) 336 h in coal ash, alkali sulfate, and NaCl mixture.

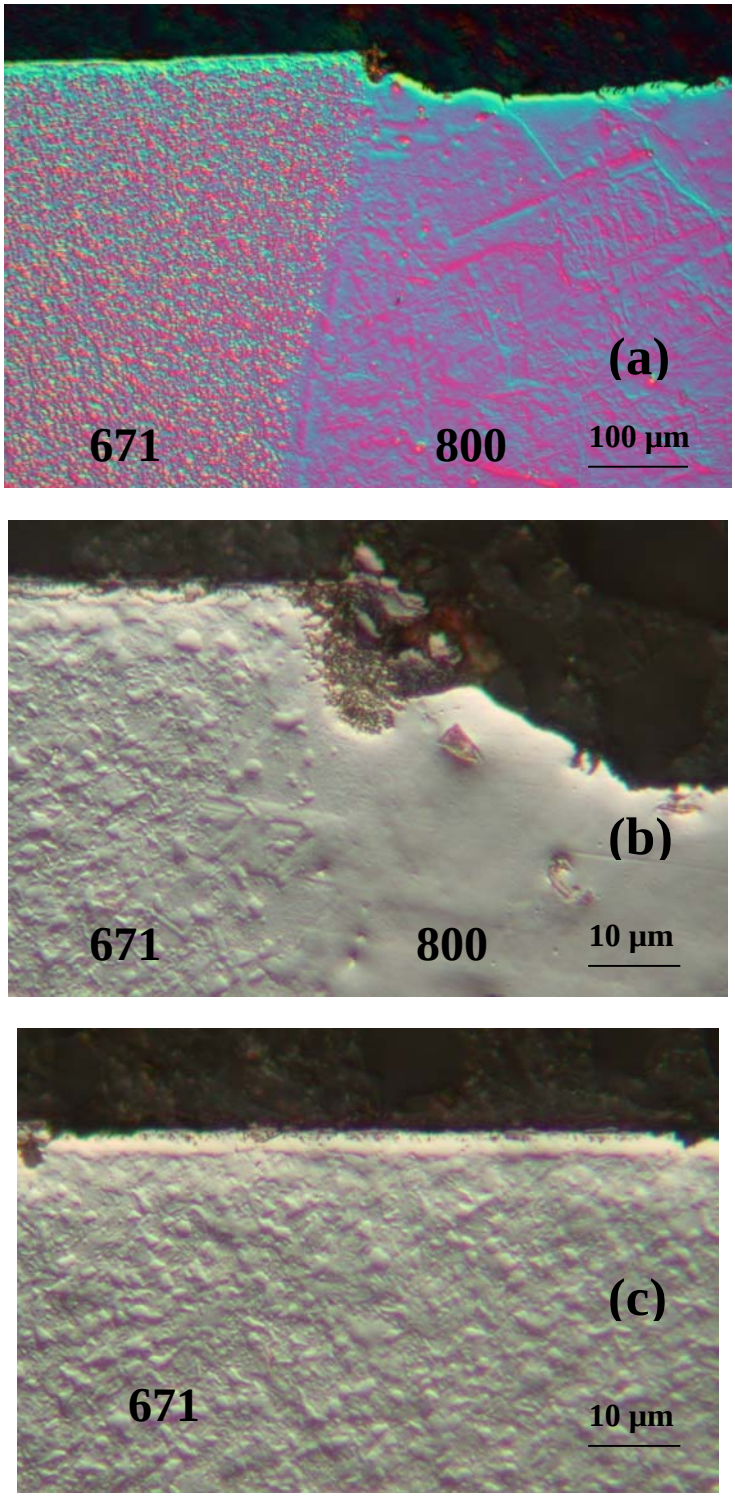

Figure 9. SEM photomicrographs of 800H clad with Alloy 671 after exposure at 650°C for 668 h in coal ash and alkali sulfate mixture (a) low magnification, (b) high magnification, and (c) clad alloy far away from interface region.

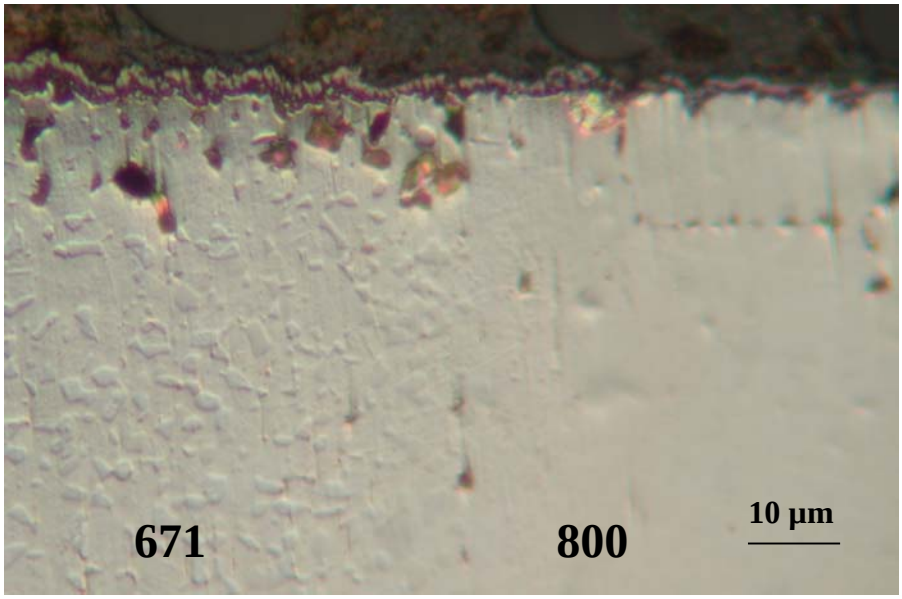

Figure 10. SEM photomicrographs of 800H clad with Alloy 671 after exposure at 800°C for 672 h in coal ash and alkali sulfate mixture.

which included ash constituents, alkali sulfates, and NaCl. Corrosion rate data showed a bell-shaped curve, with peak rates at ≈725°C, and the rate itself was dependent on the alloy chemistry. Several alloys showed acceptable rates in the sulfate-containing coal ash environment; but NaCl in the deposit led to catastrophic corrosion at 650 and 800°C. To attain acceptable corrosion, it is essential to establish maximum levels for alkali sulfates and alkali chlorides in combustion environments (and their relationship to coal feedstock). Additional tests are in progress, with less NaCl, to evaluate the corrosion performance of several Ni-base alloys. A combination of adequate creep strength, fireside corrosion resistance, and steam-side corrosion resistance is still a challenge in materials development for advanced steam cycle applications.

References

[1]. R. Viswanathan and W. Bakker, J. Mater. Eng. Perf. 10 (1), 2001, 81.
[2]. W. T. Reid, External Corrosion and Deposits, American Elsevier, New York, 1971.
[3]. E. A. Sondreal, G. H. Gronhovd, P. H. Tufte, and W. Beckering, Ash Deposits and Corrosion Due to Impurities in Combustion Gases, R. W. Bryers, ed., Hemisphere Publishing Corp., Washington DC, p. 85, 1978.
[4]. R. W. Borio and A. L. Plumley, W. R. Sylvester, ibid, p. 163.
[5]. K. Natesan and C. Reignier, Corrosion Performance of Structural Alloys in Oxygen/Sulfur/Chlorine-Containing Environments, Proc. 12th Ann. Conf. on Fossil Energy Materials, Knoxville, Paper 1.8, 1998.
[6]. K. Natesan and C. Kraus, Corrosion Performance of Structural Alloys and Coatings in the Presence of Deposits, Proc. 15th Ann. Conf. on Fossil Energy Materials, Knoxville, 2000.

Acknowledgments

This work was supported by the U.S. Department of Energy, Office of Fossil Energy, Advanced Research Materials Program, Work Breakdown Structure Element ANL–4, under Contract W–31–109–Eng–38.